Ocean–Atmosphere Covariability in the Western Arabian Sea[*]

Gabriel A. Vecchi

Joint Institute for the Study of the Atmosphere and Oceans, University of Washington, Seattle, Washington

Shang-Ping Xie

International Pacific Research Center, and Department of Meteorology, University of Hawaii at Manoa, Honolulu, Hawaii

Albert S. Fischer

Laboratoire d'Océanographie Dynamique et de Climatologie, Université Pierre et Marie Curie, Paris, France

ABSTRACT

The western Arabian Sea exhibits strong spatial variability in sea surface temperature (SST) during the southwest monsoon, with changes in SST that can exceed 5°C over 200 km. Exploration of satellite-based and in situ data shows a strong connection between mesoscale SST features and changes in the atmospheric boundary layer. The fundamental relationship is that of weak (strong) wind velocities overlying cold (warm) SST features. There are also coherent changes in other near-surface meteorological parameters, such as the air–sea temperature difference and relative humidity—indicating changes in the stability of the planetary boundary layer over the mesoscale SST features. These relationships are similar to those recently reported over the equatorial Pacific tropical instability wave region.

This observed covariability of atmospheric boundary layer structure and SST results in variations of the surface heat and moisture fluxes; latent heat flux is modified by changes in relative humidity (principally through the temperature dependence of saturation specific humidity), wind speed, and boundary layer stability over the cold filaments. The nonlinear dependence of latent heat flux on the three parameters leads to a net enhancement of latent heat flux from the mesoscale features, as compared to that computed using spatially averaged parameters.

Additionally, the spatial structure of the heat-flux variability will tend to dampen the mesoscale SST features. The mesoscale wind variability results in strong wind stress curl patterns on the same spatial scales as the oceanic features. The resulting Ekman pumping variations may play an important role in the evolution of the ocean eddy fields in this region. Further examination of the processes controlling the observed covariability, and the oceanic and atmospheric response to the coupling should therefore be undertaken.

1. Introduction

The western Arabian Sea is a region with large-scale and strong surface wind forcing during the southwest monsoon, and a vigorous dynamical ocean response that yields large SST gradients on the oceanic mesoscale. Here, we use a combination of satellite and in situ data to describe a local coupling between the surface wind and SST on the oceanic mesoscale, in which cold SSTs are associated with weak surface winds.

Corresponding author address: Dr. Gabriel A. Vecchi, NOAA/GFDL, Princeton University, Forrestal Campus, U.S. Rte. 1, P.O. Box 308, Princeton, NJ 08542.
E-mail: Gabriel.A.Vecchi@noaa.gov

The western Indian Ocean is dominated by the monsoon circulation system, which includes the largest seasonal reversals of winds and near-surface currents in the world. The existence and seasonal dependence of these wind and current shifts have been known for centuries (see Warren 1966). The dominant winds shift from being strongly northeasterly (monthly mean wind speed >7 m s^{-1}) during boreal winter months (the northeast monsoon), to being strongly southwesterly (monthly mean wind speed >13 m s^{-1}) during the boreal summer months (the southwest monsoon) (e.g., Findlater 1969, 1971).

Driven by these wind reversals, there are large changes in the ocean near-surface currents, thermal, and salinity structures in the western Indian Ocean. The southwest monsoon winds drive the intense northeastward Somali Current along the coast of Somalia, whose surface currents can exceed 200 cm s^{-1} (e.g., Swallow and Bruce 1966; Schott and Quadfasel 1982; Schott 1983).

The Somali Current develops strong eddy structures through the southwest monsoon, including the anticyclonic "Great Whirl" off the Horn of Africa (e.g., Bruce 1970; Düing 1977; Schott 1983; Schott et al. 1997), which includes a strong southwestward flow offshore of the Somali Current. Associated with these strong current and eddy structures are distinctive SST patterns, with extremely cold SSTs surrounded by warmer waters (Bruce 1974; Düing 1977; Evans and Brown 1981; Schott and Quadfasel 1982; Schott 1983); the differences between the coldest SSTs in the core of the Great Whirl wedge and the ambient waters can exceed 5°C. These extremely cold, upwelled, nutrient-rich waters are associated with variations in fish stocks (e.g., Foxton 1965).

Along the southeast coast of the Arabian peninsula, there are also distinctive cold water filaments that form during the southwest monsoon, pulling coastally upwelled water into the interior of the Arabian Sea (e.g., Bruce 1974; Manghnani et al. 1998; Morrison et al. 1998; Fischer et al. 2002). The strong seasonal variability in oceanic circulation is also associated with changes in the biological and chemical characteristics of the water column (e.g., Brink et al. 1998; Smith 1998, 1999; Ryabchenko et al. 1998).

We here report results from satellite-based and in situ measurements that describe strong ocean–atmosphere covariability linked to western Arabian Sea SST variability during the southwest monsoon. We find that during the southwest monsoon there is a strong covariability of SST and winds on the oceanic mesoscale evident across a range of time scales in the western Arabian Sea. Cold (warm) SSTs are coincident with locally weak (strong) winds. The covariability results in significant mesoscale wind stress curl and Ekman pumping patterns that may influence the mesoscale oceanic evolution in the region, as well as changes in surface moisture and heat fluxes.

Similar covariability of wind and SST has recently been reported over the strong temperature gradients associated with tropical instabilities in the eastern equatorial Pacific (Xie et al. 1998; Chelton et al. 2001a; Hashizume et al. 2001), and in the Southern Ocean (O'Neill et al. 2003). SST modulation of atmospheric stability and the resultant vertical shear adjustment as described by Wallace et al. (1989) are generally considered to be responsible for this SST–wind coupling (Hayes et al. 1989). Over warmer SSTs, the near-surface atmosphere becomes unstable, leading to enhanced vertical mixing, bringing down high winds from aloft and accelerating the surface winds. Over cold waters on the other hand, the atmospheric stability and hence the vertical wind shear increase, decelerating surface winds. In situ soundings indeed show that the atmospheric boundary layer (ABL) stabilizes over the cold and deepens over the warm phase of tropical instability waves (TIWs; Hashizume et al. 2002), in support of the Wallace et al. (1989) mechanism.

In the next section we describe the datasets and processing methods used in our investigation. In sections 3 and 4 we detail the covariability of SST and atmospheric boundary layer parameters in the western Arabian Sea, based on satellite and in situ measurements, respectively. In section 5 we offer some discussion of their potential importance. Section 6 is a summary.

2. Data and methods

a. Satellite data

We here use the daily gridded version 3 Tropical Rainfall Measuring Mission (TRMM) Microwave Imager (TMI) SST data (Wentz et al. 2000, available through Remote Sensing Systems at http://www.ssmi.com/), available on a $0.25° \times 0.25°$ grid over the global Tropics. The ascending and descending track data are each linearly interpolated in time and then averaged with each other to produce a filled dataset. The principal features of the SST variability discussed here are evident in the track data itself, and do not result from the filling or averaging technique.

Evaluation of the TMI SST data is ongoing. However, the accuracy of the TMI SST estimate in rain-free conditions is roughly 0.5°C (Wentz et al. 2000; Kummerow 2000). Recent comparisons of TMI SST estimates with moored observations of near-surface ocean temperature have found that, on greater than weekly time scales, the TMI SST successfully reproduces the character of the 1-m-depth buoy-observed temperatures in the tropical Pacific (e.g., Chelton et al. 2001a). A comparison of the TMI SST estimate over the Bay of Bengal and the Arabian Sea with moored near-surface (2.5-m depth) temperature found a strong correspondence in the evolution of the two SST estimates on greater than weekly time scales (Senan et al. 2001). The spatial structure of the SST features from TMI compares well with that from the Pathfinder Advanced Very High Resolution Radiometer (AVHRR) satellite-based infrared SST dataset [available from National Aeronautics and Space Administration (NASA) Physical Oceanography Data Access and Analysis Center, http://podaac.nasa.gov/].

We use the TMI data from 7 December 1997 to 30 June 2002. From 10 to 20 August 2001, the TRMM satellite was moved from its original orbit height of 350–402.5 km in order to extend its lifetime. Between 12 and 16 August an instrument malfunction kept the TMI from acquiring SST data. We include 2001 in our analysis because the preboost and postboost data compare well in the region and season of interest here, and because doing so gives us an additional southwest monsoon period to examine. We note that the principal results described in this analysis are insensitive to the inclusion of post-August 2001 data.

Microwave scatterometry gives us the ability to explore basin-scale modes of vector wind variability on greater than weekly time scales. We use NASA's Quick

Scatterometer (QuikSCAT) Level-3 satellite vector wind product, with each vector component (zonal and meridional) and wind speed for both ascending and descending tracks gridded on a daily, $0.25° \times 0.25°$ grid by NASA's Jet Propulsion Lab. A daily dataset for each component and for wind speed is generated by averaging the ascending and descending tracks (when they both overlap on the same day), or by using the track that is present that day. Filled datasets for each wind component and wind speed are then generated by linear interpolation in time (gaps are generally less than 4 days long). The features described in this paper are evident in the track data, and do not result from the filling or averaging technique.

Altimeters on the European Remote Sensing (ERS) and TOPEX/Poseidon (T/P) satellites measure sea surface height (SSH) deviation from its long-term mean at their nadir. There is a tradeoff between spatial and temporal resolution: T/P has a 10-day repeat orbit with a zonal spacing between ground tracks of about 3° at Arabian Sea latitudes, while these numbers are 35 days and 0.7° for ERS (Chelton et al. 2001b). We use a merged SSH dataset that takes advantage of both T/P's high temporal and ERS's high spatial resolutions (Ducet et al. 2000), available from October 1992 to July 2001 on a 0.25° grid. Monthly means are used.

b. In situ data

Data collected during the Office of Naval Research (ONR)-sponsored Forced Upper Ocean Dynamics experiment, in cooperation with the U.S. Joint Global Ocean Flux Study (JGOFS) Arabian Sea Expedition (Smith et al. 1998), provides in situ evidence of the coupled SST–wind speed response. Among the experimental components observing the dynamical evolution of the upper ocean and atmosphere were a series of regular SeaSoar surveys (Lee et al. 2000), and a moored array (Weller et al. 1998, 2002) in the north-central Arabian Sea. SeaSoar is an undulating, towed platform containing conductivity, temperature, depth, and bio-optical sensors, typically towed between 1 and 300 m below the surface. Alerted by AVHRR imagery, a survey during the 1995 southwest monsoon season (Fig. 6) captured the early evolution of a cold filamentary feature off the Omani coast (Brink et al. 1998). This same feature later made a large contribution to the upper ocean heat budget at the site of the moored array (Fischer et al. 2002), 600 km offshore.

An Improved Meteorology sensor package (IMET; Hosom et al. 1995) measuring wind speed and direction, relative humidity, barometric pressure, incoming short-wave and longwave radiation, and precipitation, was mounted on the jackstaff of the *R/V Thompson*, 16.3 m above the mean waterline. Sea surface temperature was measured in the ship intake, 4 m below the mean waterline. Air–sea fluxes were calculated using the Tropical Ocean Global Atmosphere Coupled Ocean–Atmosphere

Response Experiment (TOGA COARE) bulk formulation (Fairall et al. 1996).

The shipboard wind speed and direction measurements showed evidence of errors due to flow distortions when the superstructure of the ship was in the quadrant upwind of the sensor. These systematic errors were compensated by corrections that matched the wind speed and direction as the ship turned corners, as well as shipboard and mooring winds when the ship was in its vicinity. This provides a good level of confidence in the variability of the wind speed measurement, with less confidence in the absolute value.

3. Covariability from satellite observations

In response to the southwest monsoon (with its general downward Ekman pumping over a large portion of the Arabian Sea), the intense Somali Current forms as the western boundary current. Figure 1a shows midsummer (15 July–15 August) altimetry SSH averaged over 3 yr (1999–2001), superimposed on SST. After the current leaves the coast south of Socotra Island around 9°–10°N, it breaks into several quasi-stationary anticyclonic eddies that continue to the northeast in a chain aligned with the general mean atmospheric flow. The eddy off the Somali coast is the well-known Great Whirl, which dominates the Arabian Sea circulation. The SSH high to the northeast, centered at 9°N, 57°E, also seems to be a climatological feature, showing up in a longer-term (10 yr) average field. A third anticyclonic eddy appears farther to the east. These eddies organize the Somali upwelling into two quasi-stationary cold filaments/wedges. Near the coast, the intense upwelling keeps the water below 20°C. The Great Whirl advects this cold coastal water offshore, first eastward and then to the south. The anticyclonic eddy to the east generates a secondary cold wedge on its eastern flank.

These cold filaments are associated with marked changes in the surface wind, and this wind–SST covariability on the oceanic mesoscale is a salient feature of the western Arabian Sea during southwest monsoons observed using QuickScat and TRMM, on time scales ranging from weekly to seasonal. Figure 2 shows the main features of the covariability using August-mean TMI SST and QuickScat wind speed, for the years 1999–2002. In each case, minima in SST are overlaid by minima in wind speed, in the cold-tongue filament associated with the Great Whirl off the coast of Somalia and in the cold SST filaments extending off the coast of Oman. These features are evident independent of the averaging period, as long as it spans part of the southwest monsoon and cold eddy features are present in the SST field.

The reduction in wind speed over the cold SST filaments can exceed 2 m s^{-1}, and results in changes to both the wind divergence and curl fields. Previous studies based on sparsely distributed in situ observations depicted the Findlater jet as a smooth wind jet off the
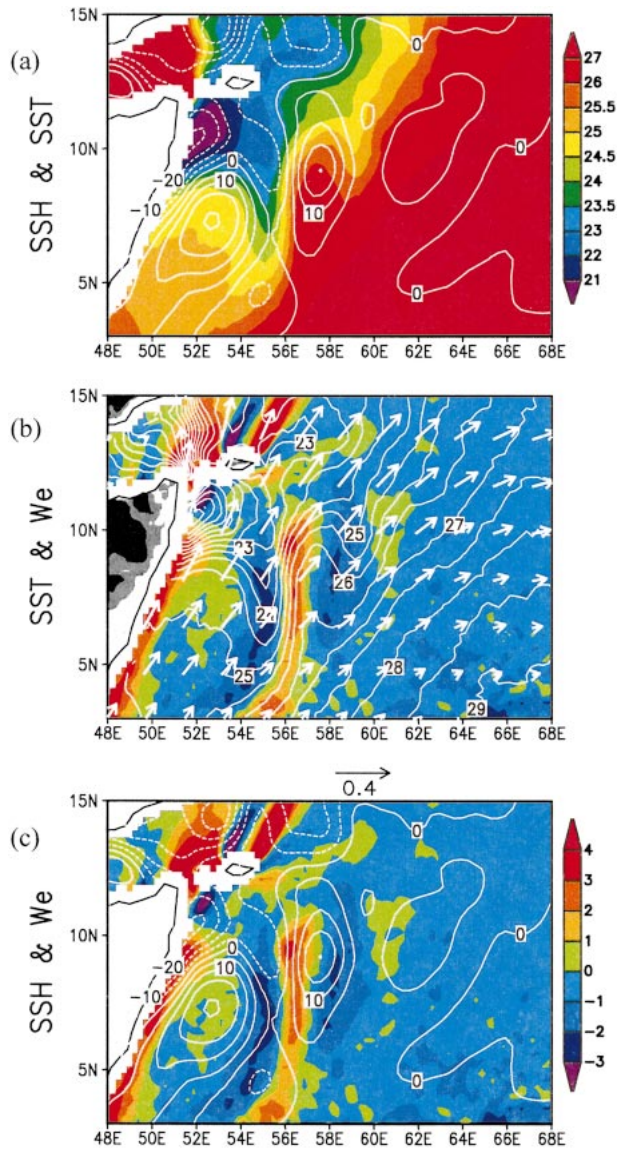
FIG. 1. Satellite-observed covariability of SST and wind speed over the Great Whirl region of the western Arabian Sea during the southwest monsoon. Socotra Island lies at 12°N, 54°E, northeast of Somalia. (a) TMI SST (shading in °C) and SSH (contours in cm); (b) SST (contours), QuikSCAT wind stress vectors (N m⁻²) and Ekman pumping velocity (shading in 10⁻⁵ m s⁻¹); (c) Ekman pumping velocity (shading) and SSH (contours), averaged for 15 Jul–15 Aug, 1999–2001. Regions with elevation greater than 300 and 600 m are gray and black, respectively, in (b).

coast of Somalia. Recent work using surface wind from a variety of satellites indicates that the Findlater jet is not a smooth feature at the ocean surface, but rather, it exhibits significant spatial variability (Halpern et al. 1999; Halpern and Woiceshyn 1999). The satellite observations presented here indicate that there is significant variability on the oceanic mesoscale in the wind jet that is associated with oceanic cold filaments, which slow down the local surface winds.

Wind stress curl features are found to be coherently associated with the mesoscale SST features. Figure 3 shows the Ekman pumping velocities from QuickScat wind stress curl with contours of TMI SST in the Great Whirl region for each southwest monsoon (1999–2002). On the windward side of the primarily meridionally oriented cold filaments there tends to be a downwelling-favorable curl pattern, while on the leeward side of the cold SST there tends to be an upwelling-favorable curl pattern. The wind stress curl patterns act on the spatial scales of the oceanic mesoscale circulation which give rise to the cold SST features. In section 5 we discuss some possible impacts of this covariability on the evolution of the mesoscale oceanic circulation of the region.

Emphasizing the covariability between wind speed and SST, Fig. 4 shows the monthly mean structure of wind speed and SST along a wind quasi-flow line, which crosses strong SST features averaged from 20 July–20 August for each of the years 1999–2002. The actual wind speed and SST are both shown, along with the high-pass along-track filtered wind speed and SST. We computed correlation coefficients between the high-passed, low-passed, and full wind and SST fields over the track, over the region 6°–20°N, for each year 1999–2002 (Table 1). The full fields do not exhibit any consistent correlation coefficient, with low values of both signs. However, the strong wind–SST correlation on the mesoscale is evident, while on larger spatial scales wind and SST are strongly anticorrelated. The statistical relationship between the low-pass-filtered fields is consistent with simple 1D mixed layer ideas of the oceanic response to wind variability: enhanced (reduced) wind speed will tend to cool (warm) the mixed layer through enhanced evaporation, vertical mixing, and entrainment; further, since the western Arabian Sea is a region of upwelling during the southwest monsoon, enhanced wind speed may increase the upwelling strength. However, the relationship between the high-pass-filtered fields is not consistent with any simple ideas of oceanic response to wind variability, and is suggestive of atmospheric boundary layer response to oceanic variability. These statistics are not sensitive to moderate changes in the averaging period or track definition.

This covariability extends in time as well as in space. Figure 5 shows distance–time sections of high-pass-filtered SST and wind speed in the southwest monsoon of 2000 along the track shown in Fig. 4. As the prevailing winds begin to turn southwesterly in May, the cold filament associated with the Great Whirl first appears on this track at 7°N, then intensifying as the season progresses, moving slowly toward the north. It becomes stationary in late June, centered at 10°N. At about the same time, the second cold filament starts to develop to the north. Both filaments begin to decay in September with the decay of the southwest monsoon. The high-passed wind anomalies copropagate northward along with the cold filament during its early development. During the entire summer, wind speed anomalies remain
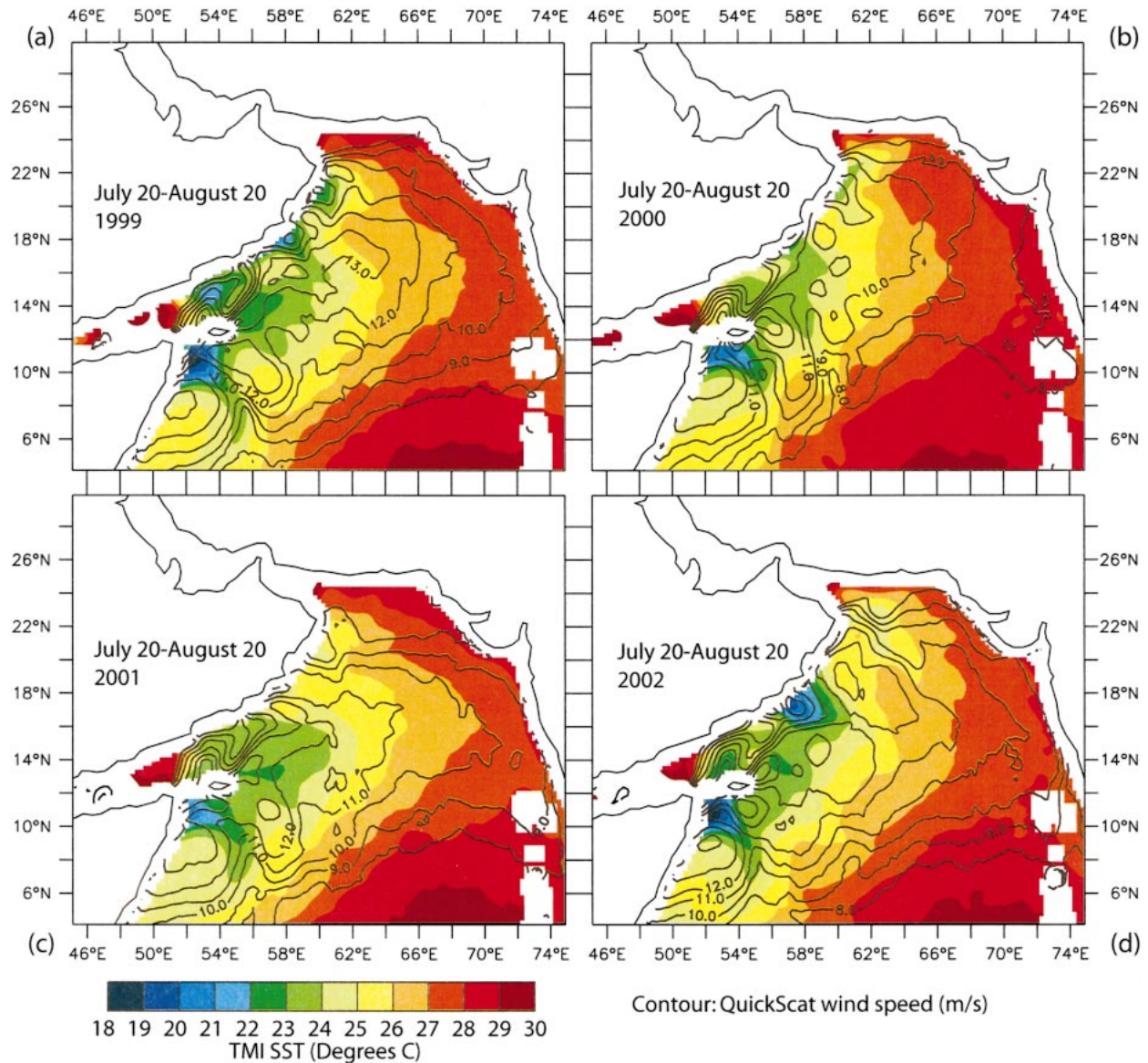
FIG. 2. Maps of SST (shaded) and wind speed (contoured) over the Arabian Sea, averaged 20 Jul–20 Aug for (a) 1999, (b) 2000, (c) 2001, and (d) 2002. SST is from TMI, units are °C. Wind speed units are m s^{-1}, with a contour interval of 1 m s^{-1}. Notice the strong covariability of wind and SST along the main axis of the Findlater jet, with locally weak winds overlying locally cold SSTs.

tightly coupled with SSTs with a positive correlation. Consistent with this in-phase relationship between the speed of the wind jet and SST, a wind curl dipole forms over the cold filament, negative on the upstream and positive on the lee side (see Fig. 3b). The coherent co-variations in space and time confirm the coupling between TMI SST and QuikSCAT wind velocity already seen in the time-mean analyses, and suggests that the mechanisms maintaining the coupling operate on time scales of days or shorter.

Scatterometers do not actually measure the wind velocity but instead the stress on the sea surface due to the relative motion of ocean and atmospheric flows. In other words, ocean currents can also exert stress/drag on the surface atmosphere. Such current signals have been detected from QuikSCAT observations both over the equatorial Pacific (Kelly et al. 2001) and over Gulf Stream rings (Cornillon and Park 2001). However, the observed structure of the covariability in the western Arabian Sea is not suggestive that the current drag is the dominant factor in its development; the stress curl would be positive over the anticyclonic ocean eddies if drag by ocean currents was dominant, but the Quik-SCAT stress curl is phase shifted in the zonal direction by almost 90° relative to the SSH anomalies. For ex-ample, positive (negative) stress curl is located west
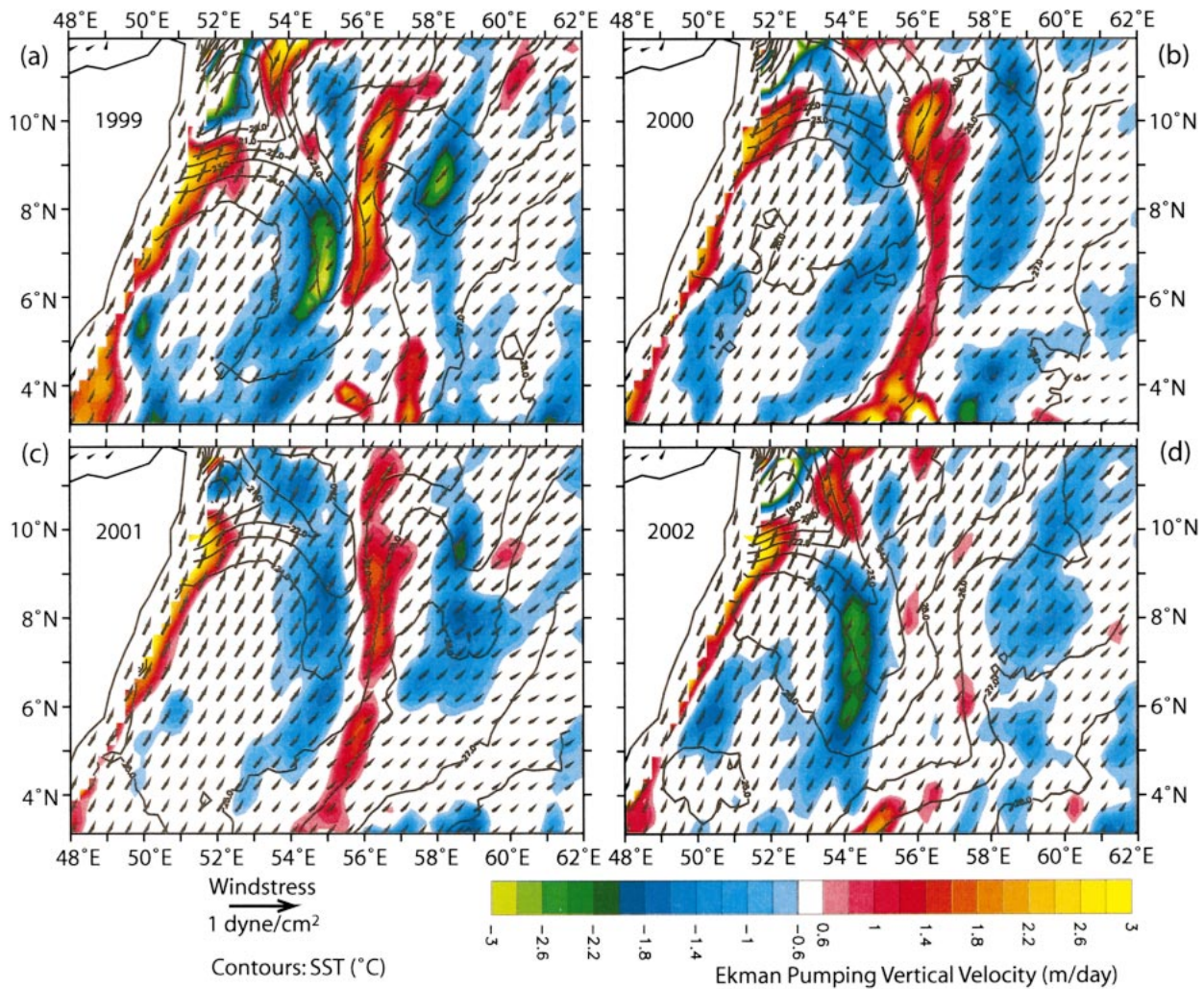
FIG. 3. Maps of SST (contour) and vertical Ekman pumping velocity (shading) over the "Great Whirl" region, averaged 20 Jul–20 Aug for (a) 1999, (b) 2000, (c) 2001, and (d) 2002. SST is from TMI, units are °C with a contour interval of 1°C. Vertical Ekman pumping velocity is computed from QuickScat winds, units are m day^{-1}, positive is upwards.

(east) of the ocean anticyclone center at 9°N, 57°E. Thus, the wind–SST covariability described here principally represents wind changes rather than current-stress variations over the western Arabian Sea.

4. Local air–sea coupling from in situ observations

In situ observations in the northwestern Arabian Sea during the southwest monsoon of 1995 offer both corroborating evidence for the satellite-observed SST–wind coupling, and indications of the mechanisms behind the observed covariability. The Findlater jet drives strong upwelling not only along the Somali coast, but along the coast of Oman, farther north. This upwelling is likewise entrained by oceanic anticyclonic features into cold filaments extending into the interior.

a. SST and wind speed covariability

Strong SST–wind coupling is observed in the outbound leg of the June 1995 SeaSoar cruise, crossing a newly developed cold filament (see Figs. 6 and 7). Sharp gradients in the along-track SST are observed as the ship moved in and out of the filament (Fig. 8, top), most notably in the first half of the trajectory over the coldest upwelled waters. These are accompanied by gradients in the observed wind speed, with stronger winds over warmer SSTs (Fig. 8, $|u|$). The correlation between wind speed and SST is 0.64 (Table 2), with the maximum contrast seen on 24 June, an increase in wind speed from about 5 to 13 m s^{-1} over an increase in SST of 3°C as the ship crossed the strong front associated with the filament. Since the SeaSoar instrument was deployed for a portion of this track, the dynamic link between the thermocline depth (as indicated by the 21°C iso-
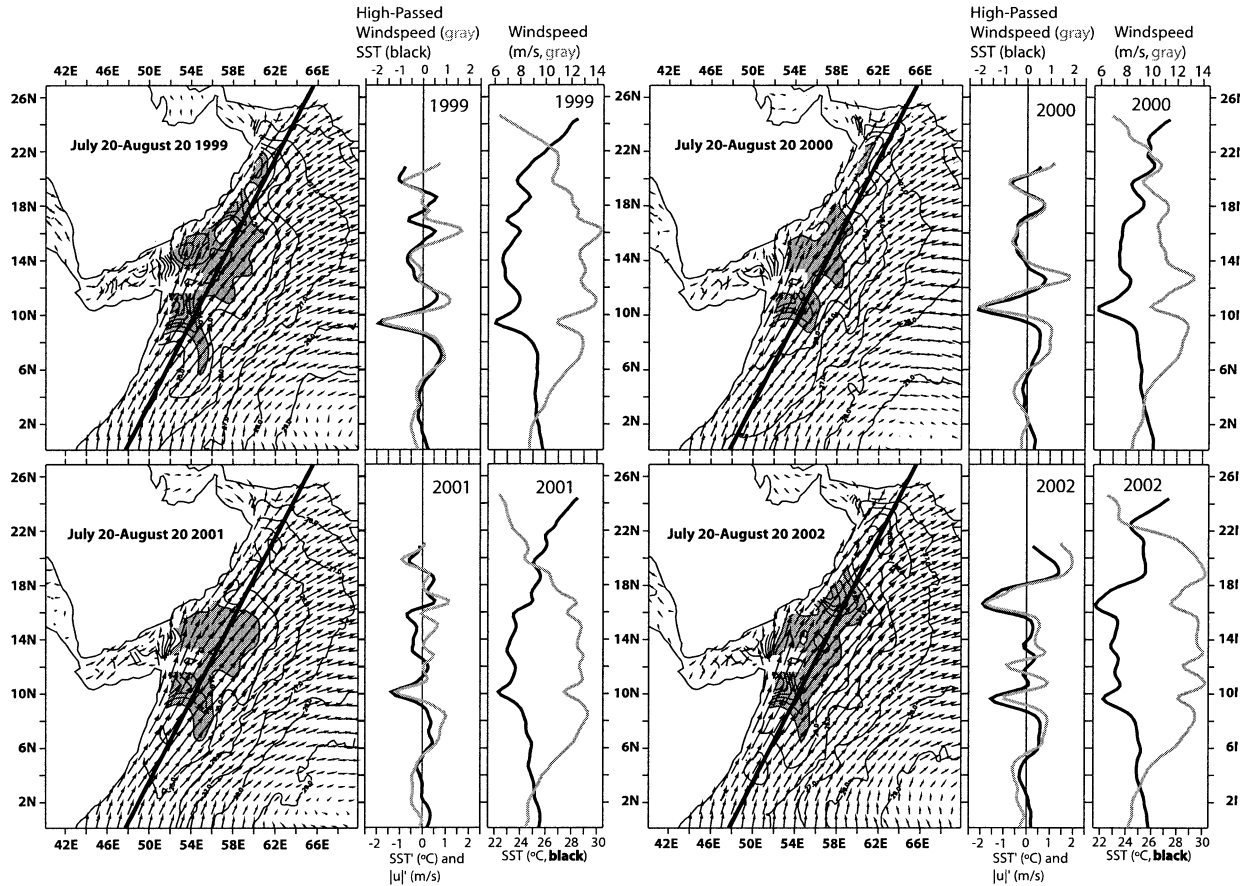
FIG. 4. Structure of "along-wind" SST from TMI and wind speed from QuickScat, and high-pass filtered SST from TMI and QuickScat averaged 20 Jul–20 Aug for each year 1999–2002. Shown for each year is an *x–y* map of the averaged SST and wind velocity, and the track along which the data are sampled. The meridional sections show, for each year, the high-pass-filtered and total wind and SST (°C) sampled along the track.

thermal surface; (Fig. 8, D21) and SST can be clearly seen, with colder SSTs associated with a movement of the thermocline closer to the surface.

b. Atmospheric stability and fluxes

The atmospheric stability and surface fluxes are also notably coupled to the SST in the observations. One indicator of the atmospheric stability is the temperature difference between the SST and the air temperature (AT), measured in the shipboard data at a height of

TABLE 1. Correlation between SST and wind speed along the track shown in Fig. 4, for high-pass-filtered, low-pass-filtered, and the full fields. Notice the consistant positive correlation for high-pass-filtered fields, and the consistant negative correlations for low-pass-filtered fields, while the full fields do not exhibit consistent correlations.

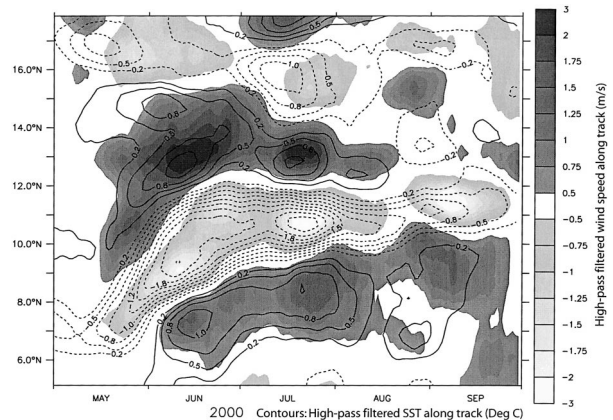| Year	High pass	Low pass	Full
1999	0.85	−0.92	0.04
2000	0.90	−0.64	0.31
2001	0.73	−0.97	−0.56
2002	0.91	−0.84	0.40

FIG. 5. Time evolution of along-wind high-pass-filtered SST (contoured, °C), wind speed (shaded, m s^{-1}) during the southwest monsoon of 2000. Evolution computed along the track shown in Fig. 4. Both fields are 15-day boxcar smoothed in time.
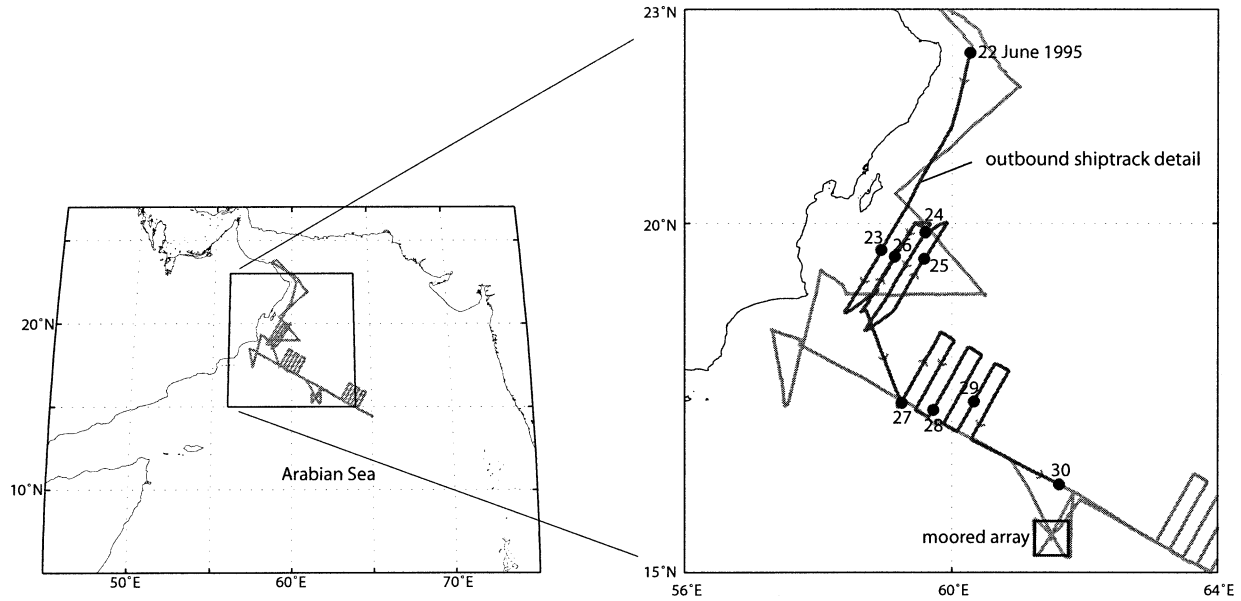
FIG. 6. Cruise track of the *R/V Thompson* off the Omani coast during the southwest monsoon, Jun–Jul 1995, with detail of the outbound leg crossing the cold filament.

16.3 m. The AT − SST difference is very small (Fig. 8, top), when away from cooler filament waters in both the shipboard and moored data (not shown). On the other hand, the drop in SST in recently upwelled waters is not fully reflected in the AT series, with an increase in the AT − SST difference over cool SSTs. Correlations between AT − SST and SST lie between 0.76 and 0.96 for various legs and periods in the shipboard and moored data (Table 2), where the air temperature sensor was 2.7 m above the mean waterline. This in-
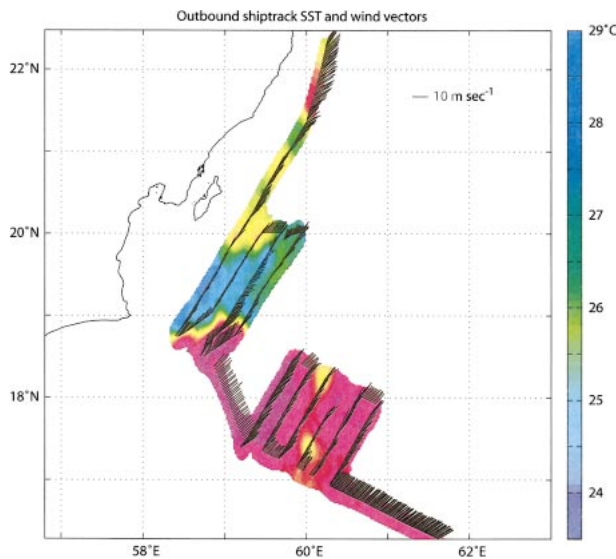

FIG. 7. Objectively mapped shipboard SST and corrected wind vectors from the outbound portion. Wind speeds are reduced over the cold feature, with the strongest gradients in both speed and direction over the SST front.
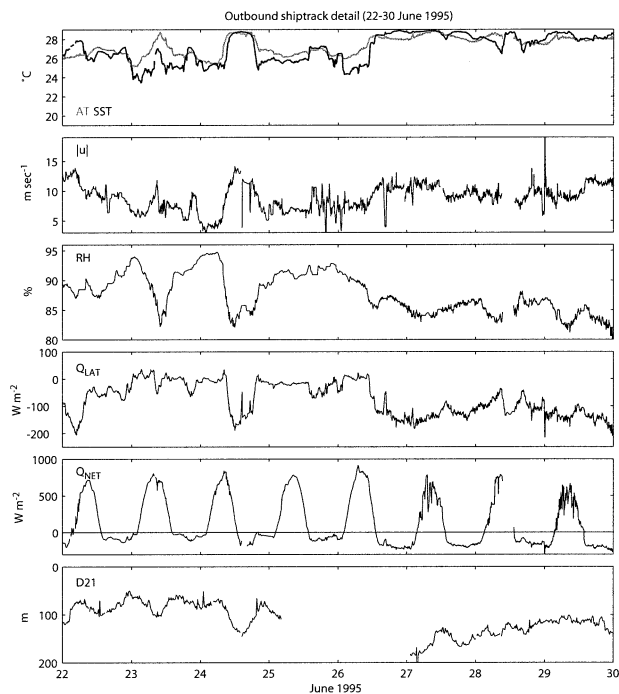

FIG. 8. (top) Outbound leg along-track observations of air temperature and sea surface temperature (AT and SST); wind speed ($|u|$), relative humidity (RH), specific humidity (q), the latent heat flux (Q_{LAT}), the net surface heat flux (Q_{NET}) and 24-hr running average, and the depth of the 21°C isotherm from the SeaSoar data (D21). Over cold water, there is a reduction in the wind speed and a near saturation of the RH, both contributing to the sharp drop in the latent heat loss. The jump in the AT − SST difference over cold SSTs suggests that the near-surface atmosphere has stratified. The colder SSTs are associated with a thermocline that is closer to the surface.

TABLE 2. Correlation coefficients between variables in the along-track outbound leg crossing into cold filamentary water.

	Q_{LAT}	$|u|$	SST
(AT − SST)	0.80	−0.44	−0.76
SST	−0.93	0.64	
$|\mathbf{u}|$	−0.78		

crease in the AT − SST difference is indicative of an increase in the stratification within the atmospheric boundary layer.

The latent heat loss associated with the strong monsoon winds is dramatically reduced over cold SSTs. There are three contributing factors: the increase in the relative humidity, the reduction in the wind speed, and the increase in the atmospheric stability. The already high relative humidity (about 85% over warm waters; (Fig. 8, RH) increases closer to the saturation point over cold SSTs, while the specific humidity has much smaller variations, on the order of the accuracy of the measurements.[1] (The accuracy in relative humidity of 4% leads to an accuracy in derived specific humidity of 0.9 g kg^{-1}.) The change in relative humidity thus appears to be in greatest part due to the drop in air temperature over the cold upwelled waters and the subsequent drop in the saturation specific humidity, rather than a change in specific humidity. As the gap between specific and saturation specific humidity closes, there is a substantial decrease in the latent heat loss (Fig. 8, Q_{LAT}), which essentially shuts down over the cold upwelled waters, and at times is even negative (indicating condensation on the sea surface). The drop in the latent heat has an effect on the daily averaged net heat flux across the air–sea boundary (Fig. 8, Q_{NET}) which increases to a heat gain for the ocean of about 200 W m^{-2} over the filament waters, as opposed to about 75 W m^{-2} over the warmer waters.

The coupled effect over the cool upwelled waters then appears to be linked to a negative thermodynamic feedback on the heat flux on the oceanic mesoscale, tending to damp out the surface SST gradient between recently upwelled and warmer surface waters. A dynamic feedback from the combined effects of increased atmospheric stability and reduced winds over the cold SSTs also exists, and is further discussed later.

---

[1] The relatively constant specific humidity appears to be maintained by a negative feedback due to vertical mixing. Over warmer waters, strong vertical mixing brings dry air from the upper ABL downwards, countering the effect of increased surface evaporation. Over cold filaments on the other hand, exchange with dry upper air is inhibited, trapping the moisture in a thinner atmospheric mixed layer. Consistent with this hypothesis, a radiosonde transect across eastern Pacific TIWs shows moistening (drying) in the upper ABL over warmer (colder) waters, with relatively small variations in surface specific humidity (Hashizume et al. 2002). This leads to an increase in column-integrated water vapor over warmer and a decrease over colder waters, a variation indeed observed by satellites (Hashizume et al. 2001).
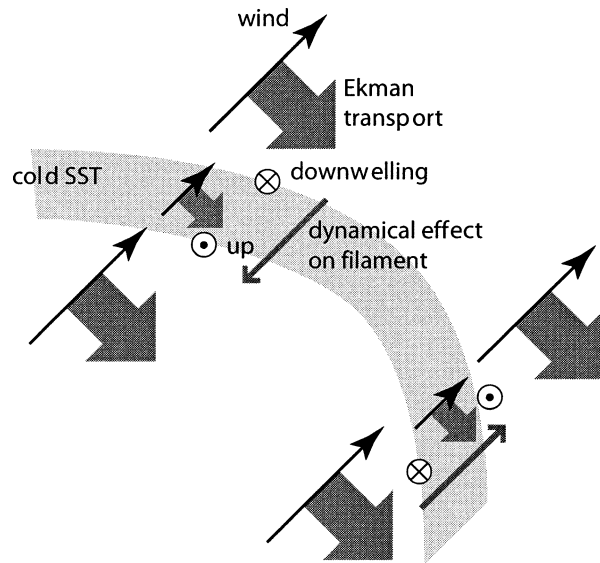

FIG. 9. Schematic of cold filaments and wind curl. Upwelling and downwelling Ekman pumping anomalies are dependent on the orientation of the filament to the mean wind direction.

Latent heat flux depends nonlinearly on three parameters, which covary with the mesoscale SST features: wind speed, relative humidity (principally through variations in saturation specific humidity), and boundary layer stability. The relationship of the impact on latent heat flux of each parameter, and the observed covariability with SST of each parameter, results in a net enhancement of latent heat flux by the mesoscale features. The spatial average of the latent heat flux computed from the high-resolution data is larger than that computed from the spatial average of the data. For the data displayed in Fig. 8, the mean of the latent heat flux is −63 W m^{-2}, while the latent heat flux of the mean observed quantities is −53 W m^{-2}. In this case, the eddy structure and covariability of the ocean–atmosphere system results in a significant modification of the net latent heat flux. We must caution that this calculation is for one realization over a strong feature, so we cannot address how representative it is. But it illustrates the potential net impact of the mesoscale covariability on latent heat flux. We cannot estimate the net effect using the satellite data, since the satellites do not measure boundary layer stability or saturation specific humidity (the dominant control of relative humidity in the in situ data).

5. Discussion

The satellite-observed zones of Ekman suction and pumping on either side of the cold SST filaments can be understood through the SST–wind speed covariance and the geometry of the relationship between the SST fronts and the mean wind. When the wind intersects an SST front at any angle but perpendicular an anomalous

Ekman vertical velocity is imposed (Fig. 9). In the case of a meridional cold SST filament and a southwesterly wind (Fig. 9, bottom; and typical in the observations on the eastern flank of the Great Whirl, Fig. 1b, Fig. 3), a strong southeastward Ekman transport is imposed in the oceanic boundary layer upwind of the SST filament. Over the filament the surface wind and Ekman transport are reduced, while downwind the wind and transport increase again. The relationship between the southeastward Ekman transports and the meridional SST gradient creates an oceanic convergence (divergence) and downwelling (upwelling) on the upwind (downwind) edge of the filament. Considering the cold features to have a thermocline pulled closer to the surface, this would tend to move the feature northeastward in this particular mean wind–SST gradient configuration. These relationships are changed if the orientation of the filament to the wind is changed (Fig. 9, top) and can be observed in estimates of the Ekman pumping velocity on the northern flank of the Great Whirl, with downward vertical velocities upwind of the meridional retroflection, and upward velocities upwind of the zonally oriented portions (see Fig. 3). This is much in line with Chelton et al.'s (2001a) analysis of eastern Pacific TIWs, which found that mesoscale wind curl anomalies are linearly proportional to crosswind SST gradient anomalies.

The climatological satellite wind estimates of the Ekman pumping velocities over cold features in the western Arabian Sea are on the order of ± 1 m day^{-1} (Fig. 1b), while for individual months they can be as large as ± 2 m day (Fig. 3), and are on the same spatial scales as the features themselves. A higher horizontal resolution might yield higher estimates for the vertical velocity; for example, the maximum 0.3 N m^{-2} wind drop over 10 km seen in the shipboard data would yield a local Ekman pumping velocity of about 10 m day^{-1} if the wind was oriented parallel to the SST front. The amplitude of the thermocline signals associated with the Omani filaments is 60 m (Fig. 6), and the amplitude of the Great Whirl thermocline signal is 60 m (Swallow and Bruce 1966). The ± 1 m day^{-1} satellite estimate gives a decay time scale of 30 days for the thermocline driven by these wind variations. Since these cold features persist on the order of a month, the Ekman pumping associated with this local mesoscale coupling could play a dynamical role in the evolution of the oceanic eddy features once they are established. Up to now attention has focused on oceanic processes in understanding the evolution of these eddy features (see Schott and McCreary 2001 for a review), we suggest, however, that this air–sea coupling be explored as a possible contributing mechanism in their evolution.

The mesoscale heat flux variations associated with the air–sea coupling are on the order of 150 W m^{-2}, giving a decay time scale of approximately 60 days for the SSTs associated with the eddies (assuming a representative 2°C temperature difference and 100-m mixed

layer depth). There is, therefore, a significant negative thermodynamic feedback on the eddy SSTs associated with this air–sea coupling. It is slightly smaller than the dynamical feedbacks from the wind stress curl variability.

The discussion thus far focuses on the SST-induced wind curl, but we note that there are other fine features of the wind curl field induced by the orography (Fig. 1b). There are substantial offshore variations in alongshore winds off Somalia, giving rise to strong offshore upwelling (see also Halpern and Woiceshyn 1999 for an analysis of wind observations by the European Remote Sensing scatterometer). The mountains in northern Somalia generate a strong wind shear and strong upwelling at the mouth of the Gulf of Aden. Under the steady southwesterlies of the southwest monsoon, the mountains on Socotra Island (maximum elevation $\sim$1500 m) generate a wind wake with a strong wind stress curl dipole on the lee side. SSTs in the wind shadow are significantly higher than on the flanks, presumably because the weak winds suppress the release of surface turbulence heat flux from the ocean surface, or reduce the amount of wind-driven vertical mixing. This Socotra wake is somewhat similar to the recently reported wake of Hawaii, in that they leave signatures in both the ocean and atmosphere. The zonally oriented wind shadow of Hawaii has been shown to generate Sverdrup gyres and permanent currents west of the Islands (Xie et al. 2001), while the dynamic implications of the northeastward-oriented Socotra wind curl dipole remain to be investigated.

6. Summary

We have found, using satellite and in situ observations, evidence for strong coupling between the ocean and the atmosphere on the oceanic mesoscale in the western Arabian Sea during the southwest monsoon. The observations show that surface winds weaken over cold SST filaments and are accompanied by zones of Ekman upwelling and downwelling on the oceanic mesoscale, which may result in a dynamic feedback into the mesoscale features. The mesoscale SST features are also associated with variations in the stability of the atmospheric boundary layer and relative humidity, resulting in variations in surface latent heat flux. These mesoscale variations in heat flux will tend toward a negative feedback with the SST features.

Our current understanding of the Arabian Sea is based mostly on sparse ship-based observations. New satellite-based microwave remote sensing is adding finer detail to this first broad-brush picture. In particular, while the Somali Current, Great Whirl, and oceanic eddy fields in the western Arabian Sea have been considered to be driven by basin-scale wind variations and internal ocean dynamics, the satellite observations presented here show that these intense currents significantly modify the local wind structure through the strong SST features which

are generated by them. The wind stress curl and heat flux variations associated with this coupling are of significant amplitude, with scaling arguments indicating that some feedback into the ocean is possible. Since these wind variations on the oceanic mesoscale may have a significant dynamical feedback onto the ocean eddies, there may be a significant—though hereto unexplored—coupled aspect to the evolution of the ocean–atmosphere system in the western Arabian Sea during the southwest monsoon.

Further, the spatially averaged latent heat flux can be significantly impacted by the mesoscale covariability of SST with wind speed, relative humidity (through temperature impacts on saturation specific humidity), and boundary layer stability. Using high-resolution in situ data, we compute the net effect of the covariability in one case to be 19% (or 10 W m^{-2}) of that computed from the spatial average of the data (-53 W m^{-2}). If this relationship is representative of that over the western Arabian Sea, the atmospheric boundary layer covariability with SST over the oceanic mesoscale represents a significant modification of latent heat flux.

Similar coupling has been seen in the TIW region of the eastern tropical Pacific (Xie et al. 1998; Chelton et al. 2001a), over the Kuroshio Extension (Nonaka and Xie 2003) and in the Southern Ocean (O'Neill et al. 2003). A principal mechanism proposed for the development of the covariability of wind and SST is the stabilization (destabilization) of the atmospheric boundary layer over the cold (warm) SSTs,[2] as described by Wallace et al. (1989) in studying the large-scale structure of the surface winds in the eastern tropical Pacific. The in situ observations in the western Arabian Sea in 1995 give us additional evidence supporting this mechanism, with the AT − SST difference systematically increasing over colder water. The extent to which this stabilization can account for the observed signal should be explored more fully. The ubiquity of this type of air–sea covariability, in the Arabian Sea region studied here and in other regions of the World Ocean, suggests that it is a general feature of the air–sea coupled system in areas of strong SST gradients. The dynamical and thermodynamic feedbacks of this covariability on the oceanic circulation of this and other regions are worth exploring further.

REFERENCES

Brink, K., and Coauthors, 1998: Monsoons boost biological productivity in the Arabian Sea. *Eos, Trans. Amer. Geophys. Union,* **79,** 168–169.

Bruce, J. G., 1970: Notes on the Somali current system during the Southwest Monsoon. *J. Geophys. Res.,* **75,** 4170–4173.

——, 1974: Some details of upwelling off the Somali and Arabian coasts. *J. Mar. Res.,* **32,** 419–423.

Chelton, D. B., and Coauthors, 2001a: Observations of coupling between surface wind stress and sea surface temperature in the eastern tropical Pacific. *J. Climate,* **14,** 1479–1498.

——, J. Ries, B. Haines, L.-L. Fu, and P. S. Callahan, 2001b: Satellite altimetry. *Satellite Altimetry and Earth Sciences,* L.-L. Fu and P. S. Callahan, Eds., Academic Press, 1–131.

Cornillon, P., and K.-A. Park, 2001: Warm core ring velocities inferred from NSCAT. *Geophys. Res. Lett.,* **28,** 575–578.

Cronin, M. F., S.-P. Xie, and H. Hashizume, 2003: Barometric pressure variations associated with eastern Pacific tropical instability waves. *J. Climate,* **16,** 3050–3057.

Ducet, N., P. Y. Le Traon, and G. Reverdin, 2000: Global high-resolution mapping of ocean circulation from TOPEX/Poseidon and ERS-1 and -2. *J. Geophys. Res.,* **105,** 19 477–19 498.

Düing, W., 1977: Large-scale eddies in the Somali current. *Geophys. Res. Lett.,* **4,** 155–158.

Evans, R. H., and O. B. Brown, 1981: Propagation of thermal fronts in the Somali current system. *Deep-Sea Res.,* **28,** 521–527.

Fairall, C. W., E. F. Bradley, D. P. Rogers, J. B. Edson, and G. S. Young, 1996: Bulk parameterization of air–sea fluxes for TOGA COARE. *J. Geophys. Res.,* **101,** 3747–3764.

Findlater, J., 1969: Interhemispheric transport of air in the lower troposphere over the western Indian Ocean. *Quart. J. Roy. Meteor. Soc.,* **95,** 400–403.

——, 1971: Monthly mean airflow at low levels over the western Indian Ocean. *Geophys. Memo.,* **115,** 53 pp.

Fischer, A. S., R. A. Weller, D. L. Rudnick, C. C. Eriksen, C. M. Lee, K. H. Brink, C. A. Fox, and R. R. Leben, 2002: Mesoscale eddies, coastal upwelling, and the upper ocean heat budget in the Arabian Sea. *Deep-Sea Res.,* **49B,** 2231–2264.

Foxton, P., 1965: A mass fish mortality on the Somali coast. *Deep-Sea Res.,* **12,** 17–19.

Halpern, D., and P. M. Woiceshyn, 1999: Onset of the Somali jet in the Arabian Sea during June 1997. *J. Geophys. Res.,* **104,** 18 041–18 046.

——, M. H. Freilich, and R. A. Weller, 1999: ECMWF and *ERS-1*

---

[2] While this vertical mixing mechanism has received some support from ABL soundings over TIWs (Hashizume et al. 2002), a recent model study suggests that the SST-induced hydrostatic pressure gradient is also an important mechanism for surface wind variability (Small et al. 2003). Recent buoy measurements have detected such TIW-induced variability in sea level pressure (Cronin et al. 2003).

surface winds over the Arabian Sea during July 1995. *J. Phys. Oceanogr.,* **29,** 1619–1623.

Hashizume, H., S.-P. Xie, W. T. Liu, and K. Takeuchi, 2001: Local and remote atmospheric response to tropical instability waves: A global view from space. *J. Geophys. Res.,* **106,** 10 173–10 185.

——, ——, M. Fujiwara, M. Shiotani, T. Watanabe, Y. Tanimoto, W. T. Liu, and K. Takeuchi, 2002: Direct observations of atmospheric boundary layer response to SST variations associated with tropical instability waves over the eastern equatorial Pacific. *J. Climate,* **15,** 3379–3393.

Hayes, S. P., M. J. McPhaden, and J. M. Wallace, 1989: The influence of sea surface temperature on surface wind in the eastern equatorial Pacific. *J. Climate,* **2,** 1500–1506.

Hosom, D. S., R. A. Weller, R. E. Payne, and K. E. Prada, 1995: The IMET (Improved Meteorology) ship and buoy systems. *J. Atmos. Oceanic Technol.,* **12,** 527–540.

Kelly, K. A., S. Dickinson, M. J. McPhaden, and G. C. Johnson, 2001: Ocean currents evident in satellite wind data. *Geophys. Res. Lett.,* **28,** 2469–2472.

Kummerow, C., and Coauthors, 2000: The status of the Tropical Rainfall Measuring Mission (TRMM) after two years in orbit. *J. Appl. Meteor.,* **39,** 1965–1982.

Lee, C. M., B. H. Jones, K. H. Brink, and A. S. Fischer, 2000: The upper-ocean response to monsoonal forcing in the Arabian Sea: Seasonal and spatial variability. *Deep-Sea Res.,* **47B,** 1177–1226.

Manghnani, V., J. M. Morrison, T. S. Hopkins, and E. Böhm, 1998: Advection of upwelled waters in the form of plumes off Oman during the Southwest Monsoon. *Deep-Sea Res.,* **45,** 2027–2052.

Morrison, J. M., L. A. Codispoti, S. Gaurin, B. Jones, V. Manghnani, and Z. Zheng, 1998: Seasonal variation of hydrographic and nutrient fields during the US JGOFS Arabian Sea Process Study. *Deep-Sea Res.,* **45B,** 2053–2101.

Nonaka, M., and S.-P. Xie, 2003: Covariations of sea surface temperature and wind over the Kuroshio and its extension: Evidence for ocean–atmospheric feedback. *J. Climate,* **16,** 1404–1413.

O'Neill, L. W., D. B. Chelton, and S. K. Esbensen, 2003: Observations of SST-induced perturbations of the mean wind stress field over the Southern Ocean. *J. Climate,* **16,** 2340–2354.

Ryabchenko, V. A., V. A. Gorchakov, and M. J. R. Fasham, 1998: Seasonal dynamics and biological productivity in the Arabian Sea euphotic zone as simulated by a three-dimensional ecosystem model. *Global Biogeochem. Cycles,* **12,** 501–530.

Schott, F., 1983: Monsoon response of the Somali Current and associated upwelling. *Progress in Oceanography,* Vol. 21, Pergamon, 357–381.

——, and D. R. Quadfasel, 1982: Variability of the Somali Current system during the onset of the southwest monsoon, 1979. *J. Phys. Oceanogr.,* **12,** 1343–1357.

——, and J. P. McCreary, 2001: The monsoon circulation of the Indian Ocean. *Progress in Oceanography,* Vol. 51, Pergamon, 1–123.

——, J. Fischer, U. Garternicht, and D. Quadfasel, 1997: Summer monsoon response of the northern Somali current, 1995. *Geophys. Res. Lett.,* **24,** 2565–2568.

Senan, R., D. S. Anith, and D. Sengupta, 2001: Validation of SST and windspeed from TRMM using North Indian Ocean moored buoy observations. Indian Institute of Science Tech. Memo. CAOS Rep. 2001AS1, Bangalore, India, 29 pp.

Small, R. J., S.-P. Xie, and Y. Wang, 2003: Numerical simulation of atmospheric response to Pacific tropical instability waves. *J. Climate,* **16,** 3722–3740.

Smith, S. L., 1998: The 1994–1996 Arabian Sea Expedition: Oceanic response to monsoonal forcing, Part 1. *Deep-Sea Res.,* **45B,** 10–11.

——, 1999: The 1994–1996 Arabian Sea Expedition: Oceanic response to monsoonal forcing. *Deep-Sea Res.,* **46B,** 8–9.

——, L. A. Codispoti, J. M. Morrison, and R. T. Barber, 1998: The 1994–1996 Arabian Sea Expedition: An integrated, interdisciplinary investigation of the response of the northwestern Indian Ocean to monsoonal forcing. *Deep-Sea Res.,* **45B,** 1905–1915.

Swallow, J. C., and J. G. Bruce, 1966: Current measurements off the Somali coast during the southwest monsoon of 1964. *Deep-Sea Res.,* **13,** 861–888.

Wallace, J. M., T. P. Mitchell, and C. Deser, 1989: The influence of sea surface temperature on surface wind in the eastern equatorial Pacific: Seasonal and interannual variability. *J. Climate,* **2,** 1492–1499.

Warren, B. A., 1966: Medieval Arab references to the seasonally varying reversing currents of the North Indian Ocean. *Deep-Sea Res.,* **13,** 167–171.

Weller, R. A., M. F. Baumgartner, S. A. Josey, A. S. Fischer, and J. C. Kindle, 1998: A one-year record of atmospheric forcing from the Arabian Sea. *Deep-Sea Res.,* **45B,** 1961–1999.

——, A. S. Fischer, D. L. Rudnick, C. C. Eriksen, T. D. Dickey, J. Marra, C. A. Fox, and R. R. Leben, 2002: Moored observations of upper ocean response to the monsoon in the Arabian Sea during 1994–1995. *Deep-Sea Res.,* **49B,** 2195–2230.

Wentz, F. J., C. Gentemann, D. Smith, and D. Chelton, 2000: Satellite measurements of sea surface temperature through clouds. *Science,* **288,** 847–850.

Xie, S.-P., M. Ishiwatari, H. Hashizume, and K. Takeuchi, 1998: Coupled ocean–atmospheric waves on the equatorial front. *Geophys. Res. Lett.,* **25,** 3863–3866.

——, W. T. Liu, Q. Liu, and M. Nonaka, 2001: Far-reaching effects of the Hawaiian Islands on the Pacific ocean–atmosphere system. *Science,* **292,** 2057–2060.